Dynamic resistance of a high-T_c coated conductor wire in a perpendicular magnetic field at 77 K

Zhenan Jiang[1], Ryuki Toyomoto[2], Naoyuki Amemiya[2], Xingyou Zhang[3], Chris W. Bumby[1]

[1] Robinson Research Institute, Victoria University of Wellington, PO BOX 33436, Petone, Lower Hutt 5046, New Zealand
[2] Department of Electrical Engineering, Graduate School of Engineering, Kyoto University, Kyoto-Daigaku-Katsura, Nishikyo, Kyoto 615-8510, Japan
[3] Callaghan Innovation, 69 Gracefield Road, Lower Hutt 5140, New Zealand

E-mail: chris.bumby@vuw.ac.nz

Abstract: Superconducting high-T_c coated conductor (CC) wires comprise a ceramic thin film with a large aspect ratio. This geometry can lead to significant dissipative losses when exposed to an alternating magnetic field. Here we report experimental measurements of the 'dynamic resistance' of commercially available SuperPower and Fujikura CC wires in an AC perpendicular field. The onset of dynamic resistance occurs at a threshold field amplitude, which is determined by the total DC transport current and the penetration field of the conductor. We show that the field-dependence of the normalised magnetisation loss provides an unambiguous value for this threshold field at zero transport current. From this insight we then obtain an expression for the dynamic resistance in perpendicular field. This approach implies a linear relationship between dynamic resistance and applied field amplitude, and also between threshold field and transport current and this is consistent with our experimental data. The analytical expression obtained yields values that closely agree with measurements obtained across a wide range of frequencies and transport currents, and for multiple CC wires produced by different wire manufacturers and with significantly differing dimensions and critical currents. We further show that at high transport currents, the measured DC resistance includes an additional non-linear term which is due to flux-flow resistance incurred by the DC transport current. This occurs once the field-dependent critical current of the wire falls below the DC transport current for part of each field cycle. Our results provide an effective and simple approach to calculating the dynamic resistance of a coated conductor wire, at current and field magnitudes consistent with those expected in superconducting machines.

Keywords: 2G HTS, dynamic resistance, ac loss, coated conductor, perpendicular magnetic field

1. Introduction

Dynamic resistance occurs in a superconductor carrying a direct electrical current whilst experiencing an applied alternating magnetic field [1-4]. This form of superconducting AC loss arises from interactions between the driven DC current and moving fluxons within the superconducting wire, which leads to a time-averaged potential drop along the wire that is proportional to the magnitude of the current [3, 4]. Dynamic resistance is a dissipative loss which presents a heat load to a cryogenic system, so accurate predictions are essential to the design of high-T_c superconducting (HTS) magnets and machines which experience AC fields [5-8]. In recent years, coated conductor HTS wire has emerged as the dominant HTS wire for next generation electrical machines, and it is therefore critically important to be able to predict dynamic losses in this type of

superconductor. Dynamic resistance has also been identified as a key underlying feature of recently reported HTS flux pump devices [9-13] in which a coated conductor stator wire is exposed to an alternating perpendicular magnetic field. Such devices are of significant interest as they eliminate the requirement for current leads connecting the magnet coil to a power supply, and thus enable an HTS magnet coil to be operated in quasi-persistent mode [14].

HTS coated conductor (CC) wire comprises a thin (typically ~1 μm) film of superconducting rare-earth barium cuprate (ReBCO) material which is supported upon a planar metal tape [15]. The results in a very high aspect ratio (a/t ~ 4000), which causes large differences in the observed AC losses for perpendicular, versus parallel, magnetic fields. In perpendicular field, the flux distribution within a CC wire closely approximates to a superconducting 'strip' of finite width $2a$, and infinitesimal thickness ($2t \rightarrow 0$) as shown in figure 1a, whilst in parallel field it can be approximated as a superconducting 'slab' of finite width $2t$, and infinite thickness, ($2a \rightarrow \infty$).

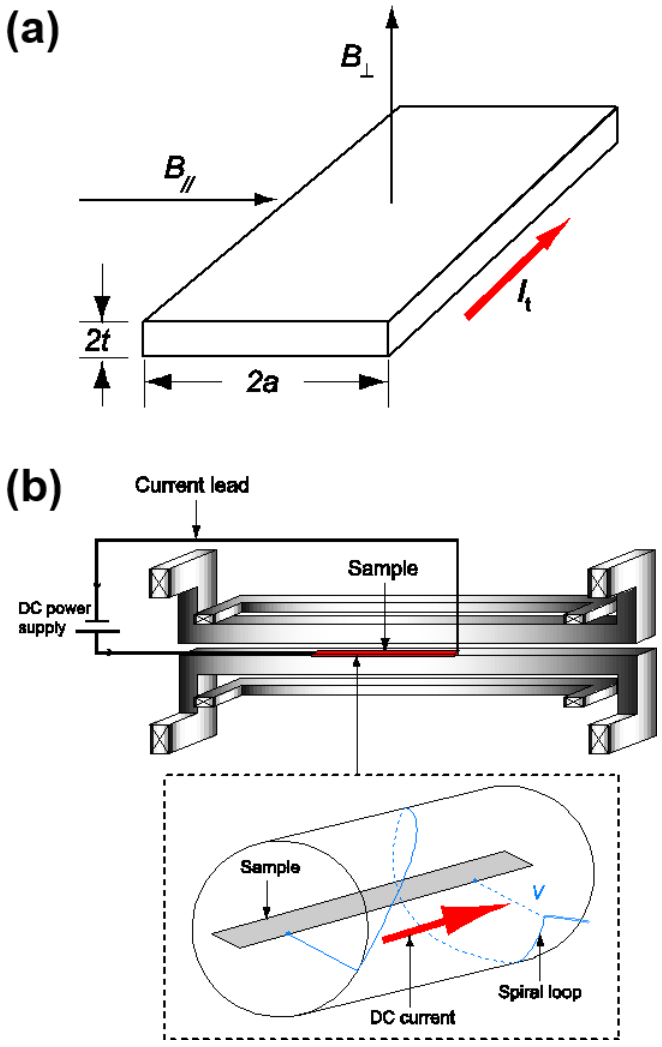

Figure 1. (a) Geometry and dimensions of superconducting strip in perpendicular field. The parameter $2t$ refers to the thickness of the ReBCO film within a coated conductor HTS wire. (b) Experimental arrangement for the measurement of dynamic resistance in a ReBCO coated conductor HTS wire. Inset shows arrangement of inductively cancelling voltage taps [16].

When either a superconducting strip or slab is exposed to an alternating magnetic field, magnetisation currents flow in the outer regions of the conductor. If the amplitude of the alternating applied field B_a, is less than a defined threshold field B_{th}, then a shielded region of "frozen flux" is maintained at the centre of the conductor [17, 18], such that any DC current flowing in this shielded region will not experience a change in the applied field. In this case, no electrical power is dissipated and the dynamic resistance is equal to zero [3, 4]. However, once the applied field exceeds B_{th}, the central region is no longer shielded throughout the entire cycle, and a net flow of flux will pass across the DC current-carrying region [4], causing dynamic resistance to occur.

For the purposes of the discussion below, we shall assume that any magnetic field dependence of J_c can be neglected, such that $J_c = J_{c0} = I_{c0}/4at$ at all times. Figures 2a and 2b show the current distribution in a strip conductor carrying a DC current I_t, whilst exposed to applied field magnitudes > $|B_{th}|$. Under these conditions, the current density is equal to J_{c0} at all points within the strip, except for a small current-reversal zone which separates the positive and negative current-carrying regions and in which $|J| < J_{c0}$. The current reversal zone has a total width, δ, which slowly decreases with increasing applied field amplitude above B_{th} [17, 18]. As in the slab case [3, 4], the constant DC transport current flows in the central region of the conductor between $y=-ia$ and $y=+ai$, where $i = I_t/I_{c0}$.

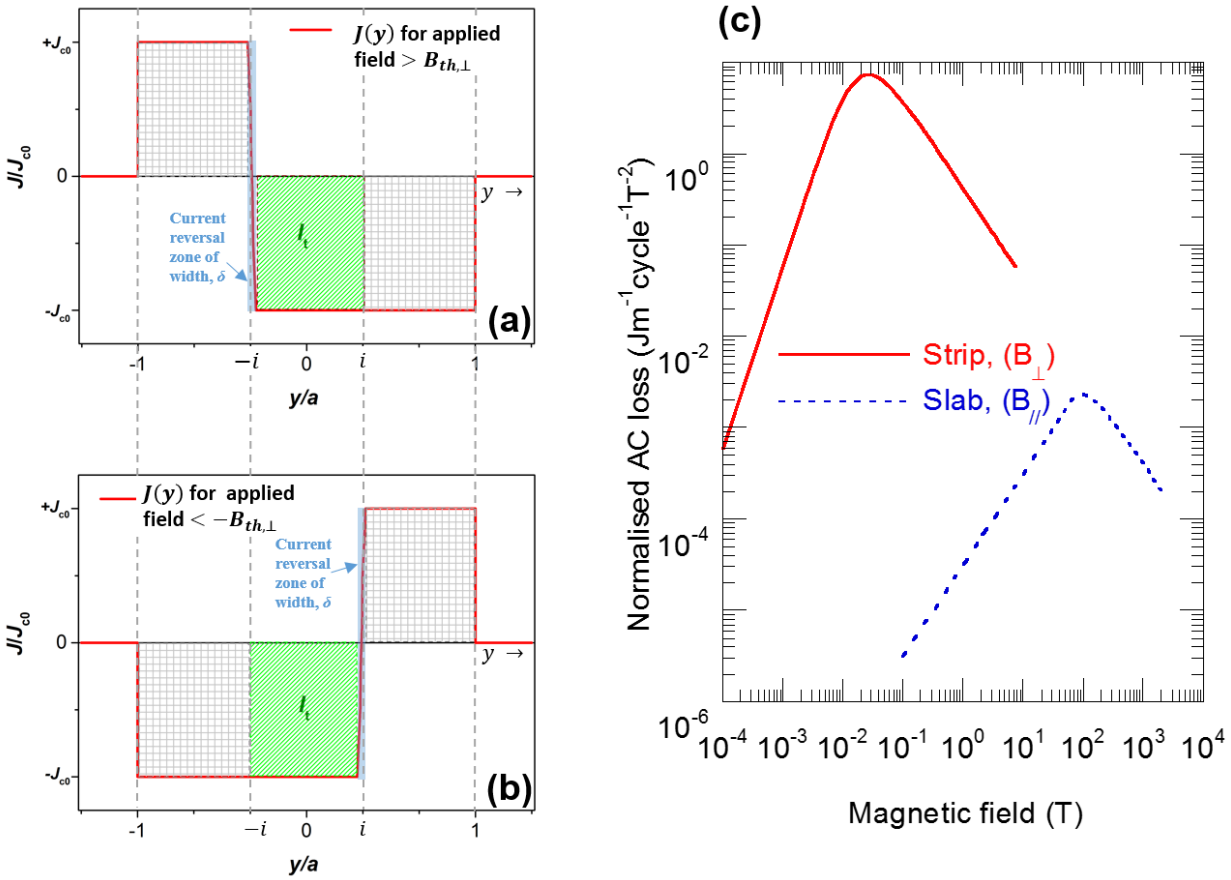

Figure 2. Diagrams (a) and (b) indicate approximate current distribution across strip for (a) positive applied fields > $B_{th,\perp}$, and (b) negative applied fields < $-B_{th,\perp}$. The DC transport current (I_t) flows within the central region of the conductor between $y=-ai$ and $y= +ai$, whilst shielding currents occupy the remainder of the conductor volume. Plot (c) shows normalised AC magnetization losses by B_a^2 according to the Brandt equation [17] and the 'Slab' model [19]. These have been calculated for example "strip" ($B_\perp$) and "slab" ($B_\parallel$) geometries. The example strip is 4 mm wide, 1 µm-thick, and has a J_{c0} of 2.63 x 10^{10} A/m^2 (equivalent to a self-field I_{c0} of 105.3 A). The slab has a width of 4 mm, is infinitely thick, and has the same J_{c0} value as the strip.

Now, the local perpendicular field at a point, y, across the strip conductor is given by [17]:

$$B_{\perp}(y) = \frac{\mu_0 t}{2\pi}\int_{-a}^{a}\frac{J(u)}{y-u}du + B_{a,\perp} \tag{1}$$

When the magnitude of the applied field is > $|B_{th}|$, the current distribution outside of the current-reversal zone does not change with field. As $\delta \ll a$, we can then state that within the DC current carrying region:

$$\begin{aligned} B_{\perp}(y) &\approx \frac{\mu_0 t}{2\pi}\int_{-a}^{a}\frac{J_{\mathrm{th}}(u)}{y-u}du + B_{\mathrm{th},\perp} + \left(B_{\mathrm{a},\perp} - B_{\mathrm{th},\perp}\right) \qquad \text{for } B_{\mathrm{a},\perp} > B_{\mathrm{th},\perp} \text{and } |y| < ai \\ &= B_{\perp}\left(y, B_{\mathrm{a}} = B_{\mathrm{th},\perp}\right) + \Delta B \end{aligned} \tag{2}$$

where $\Delta B = B_{a,\perp} - B_{\mathrm{th},\perp}$ and $J_{\mathrm{th}}(u)$ is the current distribution at the threshold field.

Now, the electrical work done when perpendicular flux, $\Delta\Phi$, crosses a current I_{t}, is given [20] by $Q = I_{\mathrm{t}}\Delta\Phi$. As such, if the applied field is alternately cycled between $-B_{\mathrm{a}}$ and $+B_{\mathrm{a}}$, the time-averaged dissipated power, P, per unit length, L, is given by:

$$P = Qf = I_{\mathrm{t}}.2aiL\Delta Bf = \frac{4afL{I_{\mathrm{t}}}^2}{I_{\mathrm{co}}}(B_{\mathrm{a}} - B_{\mathrm{th}}) \tag{3}$$

where f is the frequency of the alternating field. The dynamic resistance, $R_{\mathrm{d}\perp}$, of the strip is then obtained from $P = {I_{\mathrm{t}}}^2 R_{\mathrm{d}\perp}$, as:

$$\frac{R_{\mathrm{d}\perp}}{L} = \frac{4af}{I_{\mathrm{co}}}\left(B_{\mathrm{a},\perp} - B_{\mathrm{th},\perp}\right) \tag{4}$$

Equation 4 is equivalent to that previously derived for the slab geometry, except that the wire dimension and threshold field parameters now relate to the strip case (ie perpendicular field). In the slab geometry, Oomen *et al.* have further shown [4] that:

$$B_{\mathrm{th},\parallel} = B_{\mathrm{p},\parallel}(1 - i) \qquad \text{where} \qquad B_{\mathrm{p},\parallel} = \mu_0 J_{\mathrm{c}0} t \tag{5}$$

Here $B_{\mathrm{p},\parallel}$ is the slab penetration field, which is defined as the minimum applied field required for flux to reach the centre of a superconducting slab carrying zero transport current. Equation 5 has been shown to provide close agreement to experimental values obtained in parallel applied fields for Bi-2223/Ag wire [21]. There have also been some previous experimental studies of both Bi-2223/Ag wires [21, 22] and coated conductors [23, 24] in perpendicular magnetic field. However, attempts to adapt equation (5) to the perpendicular field data have not provided close agreement. In fact, a naïve rotation of axis such that the dimensions of width (a) and thickness (t) are interchanged in equation 5, leads to values of $B_{\mathrm{th},\perp}$ which disagree with experiment by more than 1000-fold. This then raises the question – how should we calculate the threshold field value in the strip geometry?

The threshold field, $B_{\mathrm{th},\perp}$ is the maximum field at which it is energetically-favourable for the central region of the strip to be shielded from changes in the externally applied field. In the limiting case $i \to 0$, this occurs at the maxima of the normalised hysteretic ac magnetisation loss. Figure 2c shows example plots of these curves for a slab and strip of equal width, calculated using the slab model [19], and the Brandt and Indenbom model[17, 25] respectively. This approach provides a well-defined unambiguous value for the effective penetration field of the strip, $B_{\mathrm{p},\perp}$, which describes the point at which the shielding current capacity of the strip is effectively saturated [12, 26, 27]. The maxima of the gamma function is then obtained from:

$$0 = \frac{d}{dx}\left(\frac{Q_{BI}}{H^2}\right) = \frac{d}{dx}\left(\frac{2\ln(\cosh(x))}{x^2} - \frac{\tanh(x)}{x}\right) = \frac{3\tanh(x)}{x^2} - \frac{4\ln(\cosh(x))}{x^3} - \frac{1-(\tanh(x))^2}{x} \tag{6}$$

where $x = H/H_c = B_a/B_c$ and $H_c = B_c/\mu_0 = 2tJ_{c0}/\pi$. Equation 6 can be solved by simple numerical methods to yield the unique solution, $x = 2.4642$ (to 4 d.p) and hence we obtain $B_{p,\perp} = 4.9284\mu_0 J_{c0} t/\pi$.

At values of $i > 0$, we must expect that $B_{th,\perp}$ will be lower than $B_{p,\perp}$. This is because the transport current will displace some shielding currents flowing within the strip. Furthermore, the width of the current-reversal zone δ, in the saturated current state (ie figures 2a and 2b) should remain similar to the $i = 0$ case. As δ is small, this implies that we can employ the same linear superposition of transport and shielding currents invoked in equation 5. By direct analogy, we then obtain:

$$B_{th,\perp} = \frac{4.9284\mu_0 J_{c0} t}{\pi}(1-i) \tag{7}$$

An alternative expression for $B_{th,\perp}$, has been proposed by *Ciszek et al* [23] who have transformed the parallel field value in equation 5 by a geometric demagnetisation factor [28] to obtain:

$$B_{th,\perp} = aB_{th,\parallel}/t\chi_0 = \frac{4\mu_0 J_{c0} t}{\pi}(1-i) \tag{8}$$

Equation 8 differs from equation 7 only in the magnitude of the pre-factor, $B_{p,\perp}$. However the external demagnetisation factor employed in this case does not effectively describe changes arising from the highly non-linear field profile inside the strip, which is not a simple linear transformation of the slab case.

A third approach has been taken by *Mikitik and Brandt* who have suggested that, contrary to equation 4, the threshold field should actually follow a non-linear function of i of the form [29]:

$$B_{th,\perp} = \frac{\mu_0 J_{c0} t}{2\pi}\left[\frac{1}{i}\ln\left(\frac{1+i}{1-i}\right) + \ln\left(\frac{1-i^2}{4i^2}\right)\right] \tag{9}$$

Equation 9 has not previously been tested against valid experimental data. It's derivation assumes that δ is exactly zero, and defines B_{th} as the point at which flux first passes the mid-point of the current reversal zone. It is possible that this approach may underestimate B_{th} if flux passes through the current reversal zone without subsequently traversing the DC transport current. This is because dynamic resistance will not occur if flux exits the conductor from the same side as it enters, as in that case the interactions between moving flux lines and transport current will cancel across a cycle.

In this work we have undertaken experimental measurements of the dynamic resistance in a coated conductor wire. We have then compared our results and those of previous authors, with calculated values obtained from equations 4, 7, 8 and 9.

2. Experimental method

The apparatus used to make these experimental measurements is shown in figure 1b. All measurements were undertaken at 77 K. A 15.0 cm length of CC HTS wire was placed in the uniform field region between the poles of a custom-built AC magnet [30], which was capable of generating an alternating field of 100 mT peak at frequencies up to 112.5 Hz. A 300A DC current supply was employed, and voltage taps were attached with a spacing of 5.0 cm along the wire and arranged in an induction-cancelling geometry [16]. Time-averaged DC voltage measurements were made using a Keithley 2182 nano-voltage meter with appropriate filter settings. Experimental measurements were performed on two different coated conductor

HTS wires, each of which comprised a thin film of ReBCO material ($2t$ ~ 1–2.3 μm) deposited upon a ~100 μm Hastelloy substrate. Wire A was a 4 mm wide CC HTS wire manufactured by Superpower Inc with a measured critical current I_{c0} = 105.3 A at the 1 μV/cm criterion. Wire A was coated with 20 μm-thick copper stabilisation layer on both sides of the tape. Wire B was chosen as it possessed a significantly higher critical current per unit width than Wire A. Wire B was a 5 mm wide CC HTS wire manufactured by Fujikura Ltd. with a measured critical current I_{c0} = 266.0 A at the 1 μV/cm criterion. Wire B was stabilised by a 100 μm-thick copper layer on the ReBCO film side only.

3. Experimental results

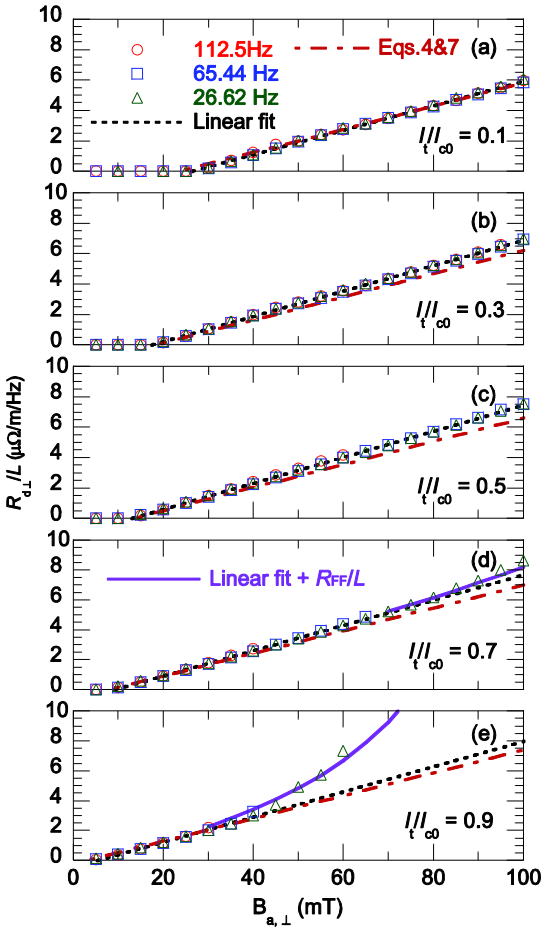

Figure 3. Comparison of $R_{d\perp}$ values measured from Wire A at 3 different frequencies and five different values of reduced current: (a) I_t/I_{c0} = 0.1; (b) I_t/I_{c0} = 0.3; (c) I_t/I_{c0} = 0.5; (d) I_t/I_{c0} = 0.7; and (e) I_t/I_{c0} = 0.9. Red dot-dashed lines show calculated values using equations 4 and 7. Black dotted lines show linear fits to experimental data (for R_d > 0.1 μΩ m^{-1} Hz^{-1}). In plot (d) the linear fit relates only to data for B_a < 80 mT, whilst in plot (e) the fit is carried out on data for B_a < 40 mT. Purple solid lines in figures (d) and (e) show sum of linear fit and R_{FF} calculated from equation 10.

Figure 3 shows experimental data obtained from Wire A at 3 different frequencies and 5 different values of reduced current, I_t/I_{c0}. In these plots $R_{d\perp}$, is normalized by f, making it clear that the loss per cycle is independent of the frequency of the alternating field. This is as expected for a hysteretic loss mechanism. Figure 3 also plots calculated values obtained using equations 4 and 7 (dot-dash red lines), which agree closely with all experimental data obtained at values of $I_t/I_{c0} \leq 0.5$. At higher transport currents and elevated field

amplitudes we observe that $R_{d\perp}$ deviates from a strict linear correlation with B_a. We believe that this can be explained by the emergence of an additional flux-flow resistance term, $R_{FF,}$ which arises once the total driven transport current exceeds the field-dependent $I_c(B_\perp)$ of the wire [31]. For an applied *B*-field of the form $B(t) = B_{a,\perp}\sin(2\pi ft)$, we can calculate the contribution of the time-averaged DC flux flow resistance, R_{FF}, from:

$$\frac{R_{FF}}{L} = f{I_t}^{n-1}\int_0^{1/f}\frac{E_0}{I_c(B)^n}dt \tag{10}$$

where the *n*-value is obtained from power-law fits [32] of experimental measurements of the *E-I* curve for the wire, and E_0 is defined as 1 μV cm^{-1}. In order to evaluate the contribution of flux-flow resistance, we have made experimental transport measurements of the *n*-value and critical current of Wire A at 77 K (using the 1 μV/cm criterion), for applied fields up to 200 mT (see supplementary material). The sum of the linear hysteretic resistance and R_{FF} has then been calculated using equation 10, and this is plotted in figures 3d and 3e where it is shown as a solid purple line for values of applied field where $I_c(B_\perp)$ falls below the DC transport current. It is clear that including this additional flux-flow resistance now provides a good description of the observed deviation from linearity at high currents.

This does provoke the question as to why equation 4 provides such an effective description of experimental results at lower transport currents, given that the derivation of equation 4 does not consider the field-dependence of $J_c(B_\perp)$. If the field-dependent contribution to $R_{d\perp}$ were not negligible, then we would expect to see deviation from linearity in the high field data obtained for $I_t/I_{c0} \leq 0.5$. We do not observe this. We suggest the success of the field-independent approach might be due to partial shielding of the central DC current-carrying region of the wire, which means that the local $J_c(B_\perp)$ at the centre of the strip is actually larger than the average value across the entire wire [33]. It is important to note that when i <1 the situation at the centre of the wire differs significantly from a transport measurement of the wire critical current, as in the latter case i =1 at the point of measurement such that shielding currents are eliminated. Similarly, the shielding effect will be reduced during dynamic resistance measurements at values of $i \rightarrow 1$. However, in this case we have observed that the field-dependence of $J_c(B_\perp)$ gives rise to a flux-flow resistance term which increases rapidly, thus dominating any underlying minor perturbations to the hysteretic $R_{d\perp}$ term.

Experimental values for $B_{th,\perp}$ were obtained from figure 3 by finding the *x*-axis intercept of linear fits (dotted straight lines in figure 3) to the composite dataset obtained at all frequencies for each value of reduced current, i. For values of $I_t/I_c \leq 0.5$, the entire dataset for $R_{d\perp} > 0.1$ μΩ m^{-1} Hz^{-1} was fitted, whilst for values of $I_t/I_{c0} > 0.5$, we have fitted only the linear section of data which occurs at lower applied field amplitudes. Our experimentally-derived values are shown in figure 4 for both of the coated conductor HTS wires measured in this work, alongside previously reported measurements from three other samples of ReBCO coated conductor wire [23, 24]. In this plot normalised values of $B_{th,\perp}/tJ_{c0}$ are shown, which enables direct comparison between results obtained from wires with different dimensions and critical currents. Figure 4 also shows calculated normalised values obtained from each of equations 7, 8 and 9.

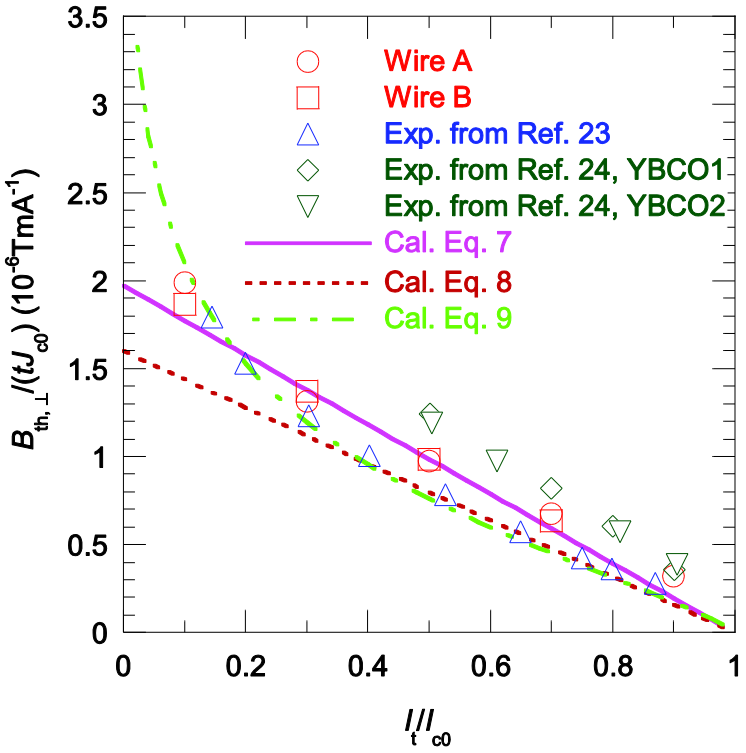

Figure 4. Plot showing normalised measured values of threshold magnetic field in perpendicular magnetic field, $B_{th,\perp}/tJ_{c0}$, versus reduced current, $i=I_t/I_{c0}$. Experimental values from this work are shown for Wire A (Superpower, I_{c0} = 105.3 A, $2a$ = 4 mm, $2t$ = 1 μm, J_{c0} = 2.63 × 10^{10} A/m^2) and Wire B (Fujikura, I_{c0} = 266.0 A, $2a$ = 5 mm, $2t$ = 2.3 μm, J_{c0} = 2.28 × 10^{10} A/m^2). Values are also shown for a single wire reported in [23] (I_{c0} = 36 A, $2a$ = 10 mm, $2t$ = 0.95 μm, J_{c0} = 3.79 × 10^9 A/m^2) and two wires reported in [24] (YBCO1: I_{c0} = 123 A, $2a$ = 4 mm, $2t$ = 1 μm, J_{c0} = 3.08 × 10^{10} A/m^2; YBCO2: I_{c0} = 91 A, $2a$ = 4 mm, $2t$ = 1 μm, J_{c0} = 2.43 × 10^{10} A/m^2). Plotted lines show calculated values obtained from each of equations 7, 8 and 9.

Our scaled experimental data agrees well with both sets of previously reported values, despite significant differences in the dimensions and critical current densities of the wires studied. In all cases we observe an approximately linearly decreasing value of $B_{th,\perp}$ with increasing i. All of the predictive equations shown (equations 7, 8, and 9) provide order-of-magnitude agreement with the measured experimental values and yield values which decrease to zero at i = 1. However, equation 7 does appear to provide the best agreement with both our own data, and the composite set of all known available data. Equation 8 appears to underestimate experimental values, whilst Equation 9 does show very close agreement with data reported in [23], but this data is not entirely consistent with the measurements made in this work and [24]. A possible reason for this might be that [23] employed a very early-generation YBCO tape of unverified homogeneity and a rather low J_{c0} (approximately a factor 10 lower than any other wire measured). In fact equations 7 and 9 yield very similar values across the experimental range plotted in figure 4, and only diverge substantially at very low reduced currents. Measurements at i <0.1 would be required to discriminate between the two equations. An additional complication arises in that the approximation δ = 0 is unlikely to be valid for very small values of I_t/I_{c0}, in which case neither equation 7 nor equation 9 should hold. However, this operating regime is of limited practical relevance to the designers of HTS machines or coils, as design engineers generally seek to make maximum use of the wire's current-carrying capacity. As such, we suggest that the simple linear expression provided by equation 7 is best suited to the estimation of dynamic resistance losses in practical systems.

4. Conclusion

Dynamic resistance in a superconductor occurs once the sum of magnetization and transport currents results in critical currents flowing throughout the entire available conductor volume. In both perpendicular and parallel field orientation, the onset of dynamic resistance in an HTS coated conductor is determined by a threshold field, B_{th} which is the minimum field amplitude at which applied flux starts to interact dissipatively with the transport current flowing in the central region of the wire.

In the perpendicular field orientation we find that $B_{th,\perp}$ decreases linearly with increasing transport current, across the full range of transport currents studied to date ($0.1 \leq i \leq 0.9$). As such, $B_{th,\perp}$ can be simply expressed as the product of a penetration field, $B_{p,\perp}$, and the transport current filling factor ($1 - I_t/I_{c0}$). The penetration field of a coated conductor in the perpendicular field case can be identified from the maxima of the normalised magnetisation loss described by Brandt and Indenbom (equation 7). We find that using this value provides calculated values of $B_{th,\perp}$ which agree closely with experimental values ($0.1 \leq i \leq 0.9$). The composite set of all available experimental data does not present any clear evidence that the more complex non-linear expression given in [29] is required to describe $B_{th,\perp}$. However, further measurements of $R_{d\perp}$ for $i < 0.1$ will be required to determine whether this remains the case in the very low current regime.

Calculated values for $B_{th,\perp}$ can be substituted into the equation derived for the dynamic resistance of a strip (equation 4), and we find very good agreement with experimental measurements of $R_{d\perp}$ for all transport currents up to $i \lesssim 0.5$. However, at higher values of i and elevated fields we find that the measured DC resistance becomes non-linear with respect to applied field amplitude. We have shown that this effect is effectively described by including an additional time-averaged flux flow term which accounts for the temporary reduction of the wire I_c below the DC transport current for a short duration in each cycle. Interestingly, this means that in the superconducting strip case, the hysteretic dynamic resistance can be described by a simple field independent model of J_c for all values of $I_t < I_c(B_{a,\perp})$.

Supplementary material

See supplementary material for experimental transport data for the wire critical current of Wire A, $I_c(B_\perp)$, as a function of applied field at 77K.

Acknowledgments

This work was supported by a grant from the Japan Society for the Promotion of Science (JSPS/OF215/005, ID No.S15728). Z.J wishes to thank Kyoto University for hosting a research visit to undertake the experimental work reported here, Nick Long for his assistance in securing this grant, and Evgeny Talantsev for I_c (B) measurement of sample wire A.

References

[1] Andrianov V V, Zenkevitch V B, Kurguzov V V, Sytchev V V, and Ternovskii F F 1970 *Sov. Phys. JETP.* **31** 815.

[2] Ogasawara K, Yasukochi K, Nose S, and Sekizawa H 1976 *Cryogenics* **17** 33.

[3] Ogasawara K, Takahashi Y, Kanbara K, Kubota Y, Yosohama K, and Yasukochi K 1979 *Cryogenics* **19** 736.

[4] Oomen M P, Rieger J, Leghissa M, ten Haken B, and ten Kate H H J 1999 *Supercond. Sci. Technol.* **12** (1999) 382.

[5] Kalsi S 2011 *Application of high temperature superconductors to electric power equipment* (IEEE Press) pp 96.

[6] Masson P J, Soban D S, Upton E, Pienkos J E, and Luongo C A, 2005 *IEEE Trans. Appl. Supercond.* **15** 2218.

[7] Pardo E 2013 *IEEE Trans. Appl. Supercond.* **24** 4700105.

[8] Barnes P N, Sumption M D, and Rhoads G L 2005 *Cryogenics* **45** 670.

[9] Geng J and Coombs T A 2015 *Appl. Phys. Lett.* **107** 142601.

[10] Geng J , Matsuda K, Fu L , Fagnard J-F , Zhang H, Zhang X, Shen B , Dong Q , Baghdadi M and Coombs T A . 2016 *J. Phys. D.: Appl. Phys.* **49** 11LT01

[11] Jiang Z, Hamilton K, Amemiya N, Badcock R A, and Bumby C W 2014 *Appl. Phys. Lett.* **105** 112601.

[12] Jiang Z, Bumby C W, Badcock R A, Sung H J, Long N J, and Amemiya N 2015 *Supercond. Sci. Technol.* **28** 115008.

[13] Bumby C W, Jiang Z, Storey J G, Pantoja A E, and Badcock R A 2016 *Appl. Phys. Lett.* **108** 122601.

[14] Bumby C W, Badcock R A, Sung H J, Kim K M, Jiang Z, Pantoja A E, Bernado P, Park M, and Buckley R G 2016 *Supercond. Sci. Technol.* **29** 024008.

[15] Selvamanickam V, Guevara A, Zhang Y, Kesgin I, Xie Y, Carota G, Chen Y, Dackow J, Zhang Y, Zuev Y, Cantoni C, Goyal A, Coulter J, and Civale L 2010 *Supercond. Sci. Technol.* **23** 014014.

[16] Fukui S, Kitoh Y, Numata T, Tsukamoto O, Fujikami J, and Hayashi K 1998 *Adv. Cryogenic. Eng.* **44** 723.

[17] Brandt E H and Indenbom M 1993 *Phys. Rev. B* **43** 12893.

[18] Zeldov E, Clem J R, McElfresh M, and Darwin M 1994 *Phys. Rev. B* **49** 9802.

[19] Wilson M 1983 *Superconducting magnets* (Oxford: Clarendon) pp 162-74.

[20] Matsushita T 1994 *Flux pinning and electromagnetic phenomenon* (Sangyo Tosho Inc. Tokyo) pp 99.

[21] Ciszek M, Knoopers H G, Rabbers J J, ten Haken B, and ten Kate H H J 2002 *Supercond. Sci. Technol.* **15** 1275.

[22] Ryu K, Song H J, Kim H J, and Seong K C 2006 *IEEE Trans. Appl. Supercond.* **15** 1011.

[23] Ciszek M, Tsukamoto O, Ogawa J, and Miyagi D, 2002 *AIP Conf. Proc.* **614** 606.

[24] Duckworth R C, Zhang Y F, Ha T, and Gouge M J 2011 *IEEE Trans. Appl. Supercond.* **21** 3251.

[25] Jiang Z, Komeda T, Amemiya N, Long N J, Staines M, Badcock R A, Bumby C and Buckley R G 2013 *Supercond. Sci. Technol.* **26** 035014.

[26] Palau A, Puig T, Obradors X, Pardo E, Navau C, Sanchez A, Usoskin A, Freyhardt H C, Fernández L, Holzapfel B, and Feenstra R 2004 *Appl. Phys. Lett.* **84** 230.

[27] Iwakuma M, Toyota K, Nigo M, Kiss T, Funaki K, Iijima Y, Saitoh T, Yamada Y, and Shiohara Y 2004 *Physica C* **412-414** 983.

[28] Fabbricatore P, Farinon S, Gomory F and Innocenti S 2000 *Supercond. Sci. Technol.* **13** 1327.

[29] Mikitik G P and Brandt E H, 2001 *Phys. Rev B* **64** 092502

[30] Jiang Z and Amemiya N 2004 *Supercond. Sci. Technol.* **17** 371.

[31] Uksusman A, Wolfus Y, Friedman A, Shaulov A, and Yeshurun Y 2009 *J. Appl. Phys.* **105** 093921.

[32] Rhyner J 1991 *Physica C* **212** 292.

[33] Sanchez A, Navau C, Del-Valle N, Chen D, and Clem J R 2010 *Appl. Phys. Lett.* **96** 072510.